Available Online

JOURNAL OF SCIENTIFIC RESEARCH

J. Sci. Res. **13** (3), 1043-1055 (2021)

www.banglajol.info/index.php/JSR

Polymeric Fe_3O_4 Conjugates with Bioactive Plant Molecules: Platforms for Antimicrobial Therapy

J. Fernandes[1], T. Vaz[1*], S. M. Gurav[2], T. S. Anvekar[1]

[1]Department of Chemistry, St. Xavier's College, Mapusa, Goa, 403507, India

[2]Department of Chemistry, Govt. College of Arts, Sc., and Com, Quepem, Goa, 403705, India

Received 3 June 2021, accepted in final revised form 29 July 2021

Abstract

The emerging nano biosystems are competent in diagnosis, drug delivery, and monitoring of therapeutic response. Both imaging and therapeutic functions can be achieved by using nanoplatforms. These nanoplatforms promise to revolutionize the medical management of many personalized illnesses. The well-developed surface chemistry of iron oxide (Fe_3O_4) makes it easy to charge them with pharmaceutics, promoting them as nanoplatforms for building up nanoparticle-based drug delivery systems. The strategy to design multifunctional Fe_3O_4 conjugates with bioactive molecules of plant origin to show enhanced activity is reported here. The conjugation reveals the magnetic Fe_3O_4 core nanoparticle surface readily link to hydroxyl sites of the Dextrin molecule, which further conjugate to conjugated with Curcumin and D-Limonene, which are powerful anti-cancer, anti-inflammatory, and antioxidant agents. The structural, morphological, optical, and magnetic properties were analyzed by X-ray diffraction, FT-Infrared, HR-Tunneling Electron Microscopy, and Vibrating Sample Magnetometer techniques. The potential drug loading was measured as Drug Entrapment Efficiency using UV-Vis spectroscopy. The antibacterial property was tested on the bacterium *S. aureus* and *E. coli*. Fe_3O_4-Dextrin nanoconjugates proved to be efficient for loading and stabilizing Curcumin and Limonene. Thus, multifunctional Fe_3O_4 conjugates are explored as exciting nano-drug carriers for targeted drug delivery.

Keywords: Fe_3O_4 nanoparticles; Dextrin; Curcumin; D-Limonene; Antimicrobial therapy; Entrapment efficiency.

doi: http://dx.doi.org/10.3329/jsr.v13i3.53740 J. Sci. Res. **13** (3), 1043-1055 (2021)

1. Introduction

Nanoscale drug delivery platforms have gained importance over the past two decades, which have shown promising clinical results in several varieties of cancer and inflammatory disorders. These nanocarriers with therapeutic loads can have minimum adverse effects. Nanoparticle materials provide potential advantages due to their unique size, physiological nature, thermal, optical, electrical, and magnetic properties, different from traditionally used materials [1-4]. A balanced perception of the relation between

* *Corresponding author*: teovaz18@gmail.com

inorganic nanomaterials and the biological system has led to the emergence of better solutions for individualized medicine. The composite organic-inorganic nanoparticles (NPs) have significantly enhanced the identification, quantification of disease biomarkers, improving the clinical trials and utility of such nanomaterials [5-7].

The uncontrollable use of antibiotics has increased the antimicrobial resistance (AMR) to medicines. The treatment of diseases has become complicated and led to high mortality rates, economic losses, worsening health care, increased diagnosis and treatment losses. Therefore, there is a search for alternative ways of treating the infections. One of the most attractive antimicrobial strategies is using the magnetic property to transport and control the release of active drugs to the diseased site. Due to the AMR to synthetic drugs, using plant compounds with antimicrobial properties is being harnessed. Drug-loaded Fe_3O_4 nanoconjugates can reach specific sites and are permeable to tissues and cells, and can deliver the forms of the inactive drug at the diseased site, minimizing the undesirable side effects [8]. Also, the toxicity effects of the drugs on healthy tissues can be avoided.

Iron oxide NPs are focused on developing novel routes for fighting diseases and infections because of their superparamagnetism and great surface/area ratio. Moreover, applications in biosystems require magnetic NPs to be stable in water at pH 7 and in the physiological environment [8]. Fe_3O_4 NPs have the potential to be used as a new antibacterial agent and are considered promising drug carriers in nanomedicine, owing to their various advantages such as biocompatibility, strong affinity, non-toxic and superparamagnetic nature [2]. As they occur naturally in the human heart, spleen, and liver, they have been approved for clinical use by FDA [8]. The well-developed surface chemistry of Fe_3O_4 makes it possible to bind them with pharmaceutics and drugs, promoting them as nanoplatforms for drug delivery. Being nanosized less amount of drug is adsorbed on the particles; thus, side effects of excess drugs can be minimized, and the exposure of the drug at the point of interest will be maximized. The release of the drug can also be controlled with respect to time and quantity [8,9]. This makes Fe_3O_4 attractive for a number of actual and potential applications in areas of biomedical applications such as in drug delivery, inhibition of microbial film and biofilm formation of many pathogens, in cancer treatments, etc. [10,11].

Dextrin (Dex) was used as a natural biocompatible organic coating to stabilize the Fe_3O_4, making them friendly to the immune system. Dex is a group of low molecular weight carbohydrates produced by hydrolysis of starch or glycogen, partially or fully water-soluble. They are mixtures of polymers of D-glucose units linked by α-(1 to 4) or α-(1 to 6) glycosidic bonds. White dextrins are used as a finishing and coating agent in pharmaceuticals.

Curcumin **(**Cur) is a biologically active, naturally occurring dietary component, which exhibits poor bioavailability due to its poor solubility in water & poor absorption. It has generated huge interest for its potential to combat human diseases such as cancer, inflammation, and cardiovascular ailments. It has been established that it acts through the phenolic hydroxyl group and the free radical scavenging mechanism is due to its nature of free-radical itself [12]. Its antioxidant property is indirectly linked to its tumor suppressant

therapy. Since it acts as an anti-cancer agent, it can work efficiently if delivered on-site by Fe_3O_4 conjugations [10-13].

D-Limonene (Lim), a natural essential oil nutrient, is a monoterpene and has potent antioxidant, anti-inflammatory, anti-cancer properties. It assists with various metabolic and health problems; safe in high doses, and helps in weight management. It is considered a superior nutrient for breast cancer prevention. Due to its many benefits, Lim can be used by any person as part of a general health program. However, due to its insolubility in water, its biological availability for enhanced effects towards various diseases becomes negligible. Thus, to avoid the troubles of negligible solubility and low bioaccessibility of Cur and Lim, these can be conjugated on iron oxide NPs. Their effects can be enhanced for their use in drug delivery and antimicrobial approaches [13,14].

In order to confer colloidal stability to the Fe_3O_4, hydrophilic and biocompatible polymers are added during the particle formation process, passing the nanocrystal surface and protecting against the agglomeration of particles. The coating gives stability, prevents oxidation, and makes the particles biocompatible. In addition, polymer coatings offer multiple chemical groups that are essential for the coupling of functional species. The coating increases longer blood circulation time and maximizes the possibility of the drug reaching the target tissues. Most importantly, the coatings serve as a base for a further anchoring of the drugs, antibodies, biomarkers, etc. to the superparamagnetic Fe_3O_4, and these bioactive drugs can then be delivered to the diseased site in the biosystems using the external magnetic field for various biomedical applications [15-17].

The objectives of this investigation were to synthesize Dex coated Fe_3O_4 nanoconjugates and then payload them with plant-derived bioactive drugs Cur and Lim. Upon characterization and confirming its structural morphology, the percentage of drug loading was studied using UV-Vis spectroscopy. The enhanced microbial activity of these drugs was then evaluated on *E. coli* and *S. aureus.*

2. Materials and Methods

All materials used were of AR grade unless specified. Distilled deionized (DI) and nitrogen purged water were used to prepare all the solutions. Reagents used were $FeCl_3 \cdot 6H_2O$ (99 % pure), $FeSO_4 \cdot 7H_2O$ (98.5 % pure), NaOH (LR), Dextrin white 99 % (Loba Chemie), Curcumin crystalline (LR) 99 %, D-Limonene >95 % (TCI, M.W. 136.24) were used as procured.

2.1. *Synthesis of Fe_3O_4 nanoparticles*

$FeCl_3 \cdot 6H_2O$ and $FeSO_4 \cdot 7H_2O$ were taken in the ratio of 2:1 and dissolved in acidified deionized water. Then 2 M NaOH was added dropwise, with constant stirring, and the reaction temperature was maintained at 60 °C. The pH was maintained above 11. The black precipitate of Fe_3O_4 obtained was sonicated for 1 h, repeatedly washed with deionized water and ethanol, and finally separated and dried. The net reaction is:

$$2Fe^{+3} + Fe^{+2} + 4OH^- \longrightarrow Fe_3O_4 + 4H^+$$

2.2. *Synthesis of Fe_3O_4-Dextrin*

Dextrin solution (20 g in 200 mL of DI water) was heated at 90 °C for 1 h with continuous agitation (200 rot/min). To this, 5 M NaOH (100 mL) was added. Iron oxide solution (100 mL) in the ratio of 1:2 ($FeSO_4 \cdot 7H_2O$ and $FeCl_3 \cdot 6H_2O$) was added dropwise to this solution. The suspension was incubated for 1 h at 90°C with gentle stirring, as reported elsewhere [18]. The reaction pH was maintained above 11 by adding 5 M NaOH solution. The black solid was washed, separated, and dried at 50 °C.

2.3. *Drug loading on synthesized Fe_3O_4-Dex to prepare Fe_3O_4-Dex-Cur and Fe_3O_4-Dex-Lim nanoconjugates*

The Fe_3O_4 was then functionalized with bioactive plant-derived drugs Cur and Lim to prepare the double-layered core/shell/secondary shell nanomaterials. Cur solution (20 mg/mL in ethanol) and Lim solution (1 mL/5 mL in ethanol) were prepared and added to a known quantity of Fe_3O_4–Dex compounds. The suspensions were stirred for several hours, allowed to settle overnight, separated, and dried. The leftover liquid was decanted off, and the amount of unused drug was quantified using UV-Visible spectroscopy [10-13]. The drugs were attached to Fe_3O_4-Dex by adsorption.

3. Results and Discussion

3.1. *Structural morphology and particle size*

X-ray powder diffraction patterns were used to determine the crystal structure and particle size in the 2Θ range of 20°-70°, recorded on Philips XRD diffractometer (PW 1840, Netherland). All the diffraction peaks were analyzed and indexed using JCPDS files and compared with magnetite standards. Fig. 1 shows the XRD pattern of all the Fe_3O_4 conjugates. Crystallite size measurements were determined from the full width at half maxima (FWHM) of the strongest reflection of (311) peak using the Debye-Scherrer approximation formula, which assumes the small crystallite size cause of line broadening. The crystallite sizes calculated are given in Table 1.

The purity and nanoconjugates in nanosize were essential, which was confirmed by studying structural morphology and particle size. There was no characteristic peak for impurities, confirming that all the compounds prepared were pure. The lattice constant *a* was found to be 8.11 Å and the diffraction peaks indexed as planes with d_{hkl} (220), (311), (400), (422), (511), and (440) stands for cubic unit cell, characteristic, and confirming the formation of cubic inverse spinel crystal system of the Fe_3O_4 structure, with the strongest reflection at (311). No shift in the peak positions in all the XRD patterns was observed, which confirms that the binding process did not result in the phase change of the MNPs [19]. The size falls in the nanometer range, confirming the formation of Fe_3O_4 nanoparticles. Table 1 illustrates that the crystallite particle size gradually decreases from 23 to 18 nm with the loading of Dex as stabilizing layer on

Fe_3O_4 and further with Cur and Lim. It is also observed that in the coated Fe_3O_4 nanocomposites, the peak intensities are weakened, and peak width is broadened, which confirms the attachment of the coating agent on the Fe_3O_4. In drug-loaded Fe_3O_4, the peak intensity further decreases, which is attributed to the fact that there is amorphous property and bilayer coverage, indicating the presence of coatings. Broad diffraction peaks in the XRD pattern of coated Fe_3O_4 also indicate a further decrease in particle size as the size decreases after coating due to reduced agglomeration.

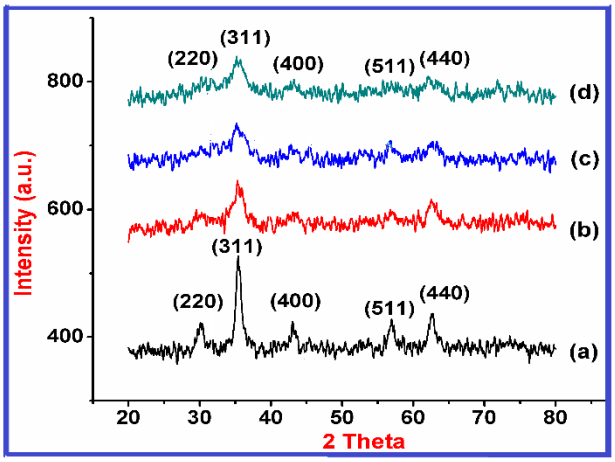

Fig. 1. Representing XRD patterns of multifunctional Fe_3O_4 materials, a) Fe_3O_4, b) Fe_3O_4-Dex, c) Fe_3O_4-Dex-Cur, and d) Fe_3O_4-Dex-Lim.

Table 1. Particle size of multifunctional Fe_3O_4 materials.

Sample No	Sample	Particle size $D = \frac{k \times \lambda}{\beta \times \cos(\Theta)}$ (Debye--Scherrer Formula)
1	Fe_3O_4	27.82 nm
2	Fe_3O_4 – Dex	22.88 nm
3	Fe_3O_4 – Dex-Cur	18.91 nm
4	Fe_3O_4 –Dex-Lim	19.80 nm

3.2. *FTIR spectroscopy*

FTIR was recorded of the dried samples using Shimadzu FTIR (8101A, Japan) instrument in the range of 4400 to 400 cm^{-1}, in the % Transmittance mode. Fig. 2 shows the FTIR spectra of Fe_3O_4, Fe_3O_4-Dex, Fe_3O_4-Dex-Cur and Fe_3O_4-Dex-Lim. The absorption peak frequencies for all the peak intensities are summarized in Table 2.

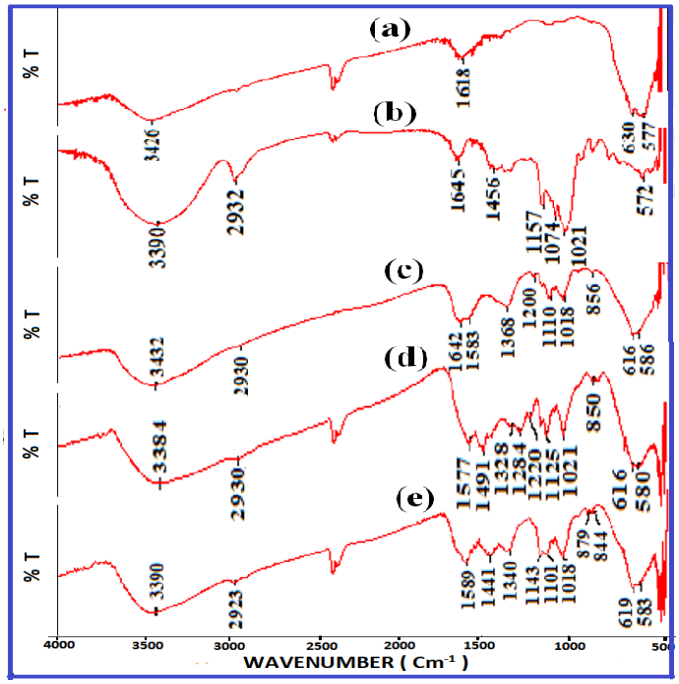

Fig. 2. FTIR absorption spectra of a) Fe_3O_4, b) Dex, c) Fe_3O_4-Dex, d) Fe_3O_4-Dex-Cur, and e) Fe_3O_4-Dex-Lim.

Table 2. Assignments of the absorption bands in the IR spectra (cm^{-1}).

Dex cm^{-1}	Fe-Dex cm^{-1}	Fe-Dex-Cur cm^{-1}	Fe-Dex-Lim cm^{-1}	Fe-O cm^{-1}	Assignments
3500-3200	3432	3381 broads	3390	3435 -OH grps attached to core	V* H-O
2925	2929	2929	2923	-	V*asy C-H of CH_2
1455, 1370	1612, 1358	1577, 1491, 1329	1642, 1589, 1441, 1340	1621-H-O-H of adsorbed water	Delta *H-C-OH, C=Ostretching
1277	1201	1284, 1219	1220	-	Delta *H-C-OH
1152	1109	1124	1148,1101	-	V*s C-O-C
800- 1200	855, 1018	849, 1021	879, 1018	-	C-C
	615, 586	615, 580	618, 583	620, 568	Fe_{td}-O-Fe_{oh}& Fe_{td}-Fe_{oh}

FT-IR spectra have provided structural insight into the nanoconjugates molecules and confirm the loading of biomolecules on Fe_3O_4 NPs. The characteristic peaks confirm the formation of Fe_3O_4 NPs and coated Fe_3O_4 conjugates. Additional peaks and broadening are observed in drug-loaded Fe_3O_4, confirming the presence of Dex, Cur and Lim. The weak intensity of the IR peaks indicates that the interactions between the Fe_3O_4 and the coating substances are of an intermolecular type.

The H-O-H bending vibration peaks of H_2O seen in the 1000-1600 cm^{-1} are a little intense. The Fe_3O_4 materials exhibit two characteristic peaks in the range 690 to 550 cm^{-1},

assigned to metal-oxygen bonding in the Fe_3O_4 crystal lattice and represent the stretching vibrations bands related to the metal octahedral and tetrahedral sites, respectively in the spinel oxide structure. The peak observed at 3435 cm^{-1} for Fe_3O_4 material relates to –OH groups and H_2O groups on the surface of Fe_3O_4 particles. The peak of Fe_3O_4 appeared at 3435 cm^{-1} shifts to 3432, 3381, and 3390 cm^{-1} in the coated samples of Fe-Dex, Dex-Cur and Dex-Lim, respectively. The shift indicates the interaction between Dex, Cur and Lim on the bare Fe_3O_4, in agreement with the literature [9,20]. The peaks at 2918 and 2849 cm^{-1} observed show the C-H stretching vibration. Some new peaks appear in the coated Fe_3O_4 and broaden some peaks, indicating the reaction between Dex and Fe_3O_4. When Fe_3O_4-Dex was coated with Cur and Lim, assignments are shifted for all the peaks. A shift in the Fe-O band is also observed. Thus, it could be confirmed that Dex, Cur, and Lim were attached to the Fe_3O_4 successfully. The negative charges on the Fe_3O_4 surface had an affinity for Dex and protonated it; thus, the coating occurred by electrostatic interactions. No impurity peaks were observed in any of the spectra, showing all the compounds formed were pure. The spectra were matched with standard literature data [9,20].

3.3. *Magnetic measurements*

Superparamagnetism plays a key role in targeting carriers in biomedical applications, and the lack of hysteresis is one criterion to identify the product as superparamagnetic. The magnetic characterization was done using a vibrating sample magnetometer at room temperature, with a magnetic field in the range of -15000 to +15000 Oe. The parameters obtained from the hysteresis loops were saturation magnetization (Ms), remanence magnetization (Mr), and Coercivity (Hc). Fig. 3 shows the VSM spectra of Fe_3O_4, Fe_3O_4-Dex, Fe_3O_4-Dex-Cur, Fe_3O_4-Dex-Lim. The Ms values are shown in Table 3.

The absence of a hysteresis loop in all the graphs confirms that the samples are superparamagnetic. Such materials have high Ms and zero coercivity and remanence magnetization. The magnetic moment of the particles, in the presence of magnetic field H, will try to align with the magnetic field direction, leading to a macroscopic magnetization of the compounds. The magnetization approached saturation when the magnetic field increased to 15000 Oe. The Ms values depend on the synthesis method and particle size. The Ms value of Fe_3O_4 is high and matches well with standard magnetite values. The Ms values of coated Fe_3O_4 decrease, confirming the presence of coatings on the Fe_3O_4. On coating of NPs, the particle size decreases, and thus Ms value also decreases, which is attributed to the incorporation of iron oxide NPs into Dex-Cur and Dex-Lim systems, which added a thick polymer layer on the particle surface [19]. This observation could also be because the particles might be assumed to have a single magnetic domain, therefore decreased Ms values. However, this amount of Ms is sufficient for biological applications for their use as drug delivery agents under applying an external magnetic field in biomedicine.

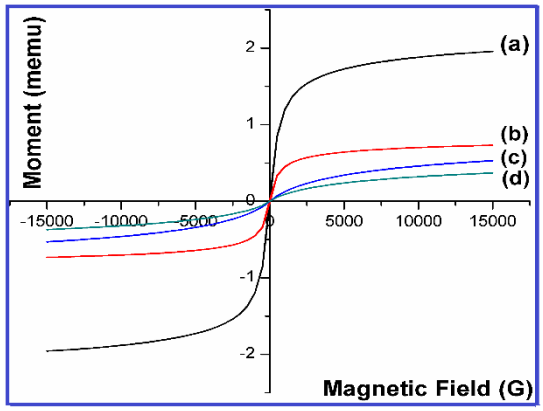

Fig. 3. VSM graphs of a) Fe_3O_4, b) Fe_3O_4-Dex, c) Fe_3O_4-Dex-Cur, and d) Fe_3O_4-Dex-Lim.

Table 3. Ms values of Fe_3O_4 samples.

Sample no	Sample	Saturation magnetization Ms emu/g
(a)	Fe_3O_4	51.47 emu/g
(b)	Fe_3O_4-Dex	20.91emu/g
(c)	Fe_3O_4-Dex-Cur	16.78 emu/g
(d)	Fe_3O_4-Dex-Lim	12.92 emu/g

3.4. *High-resolution transmission electron microscopy (HRTEM)*

Fig. 4 depicts the HRTEM images of pure Fe_3O_4 NPs and coated conjugates, taken on the JOEL JEM 2100F instrument, with an accelerating potential of 200 kV. TEM analysis revealed that the mean core size of a) Fe_3O_4 NPs was 4.30-12.78 nm, b) Fe_3O_4-Dex was 4.44-7.43 nm, c) $_{Fe3}O_4$-Dex-Cur was 6.62-13.88 nm, and that of d) Fe_3O_4-Dex-Lim was 7.64-13.98 nm, which is much lesser than that of crystallite particle size calculated with XRD technique in agreement with the literature [20,22]. As expected, the TEM particle size was smaller for the conjugate nanomaterials. Such small sizes are of great help as the drug-loaded Fe_3O_4 NPs enable the passive tissue targeting due to enhanced permeability, sustained release, and retention capacity upon administration. In addition, it is also possible to obtain the desired fine-tune ratio of hydrophilic and hydrophobic nature of conjugates, besides can manipulate the particle size and optimize the delivery efficiency [14]. The degree of agglomeration decreased after coating with Dex, Cur, and Lim, showing spherical-shaped monodispersed particles. The images show the amorphous nature of particles due to the presence of the organic coating on them.

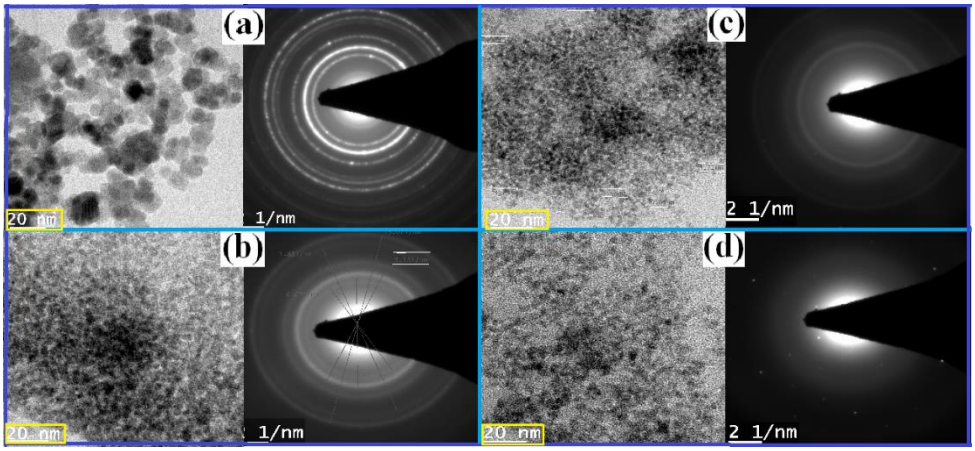

Fig. 4. TEM graphs of a) Fe_3O_4 NPs, b) Fe_3O_4-Dex, c) Fe_3O_4-Dex-Cur, and d) Fe_3O_4-Dex-Lim.

3.5. *Antimicrobial activity*

Antimicrobial tests by the Zone of Inhibition (ZI) method were carried out to quantitatively determine the inhibition of the bacterium by the bioactive plant drugs Cur and Lim loaded on the prepared Fe_3O_4-Dex. Borewell and Filter paper disc method using agar diffusion was used. The temperature and time duration of incubation was maintained at 37 °C for 24 h. The bacteria under study were *E. Coli* and *S. aureus* [22,23]. The tests were carried out using an aqueous dispersion of all the prepared conjugates, and Cur and Lim were also used as an aqueous dispersion.

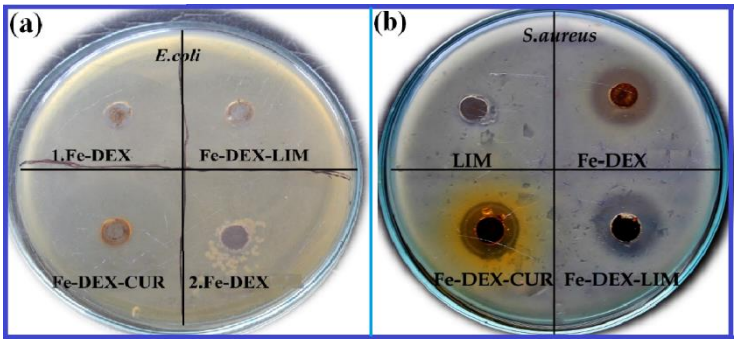

Fig. 5. Antimicrobial studies by the Zone of Inhibition (ZI) method on a) Fe_3O_4 NPs, b) Fe_3O_4-Dex, c) Fe_3O_4-Dex-Cur, and d) Fe_3O_4-Dex-Lim.

Table 4. Zone of Inhibition for (a) references/controls and (b) Fe_3O_4-Dex nanoconjugates.

	Sample	Zone of Inhibition *E. coli*	Zone of Inhibition *S. aureus*
(a)	Fe_3O_4	0	0
	Dex	0	0
	Cur	13	12
	Lim	12	11
(b)	Fe_3O_4	0	0
	Fe_3O_4-Dex	0	0
	Fe_3O_4-Dex-Cur	32 mm	21 mm
	Fe_3O_4-Dex-Lim	31 mm	23 mm

Antimicrobial tests by the Zone of Inhibition (ZI) method as crucial studies were carried out to quantitatively determine the level of inhibition of the bacterium by the nanoconjugates under investigation. The bacteria under study were commonly found in *E. coli* and *S. aureus.* The ZI reveals the efficacy of the drug molecules on the selected bacterium. It is seen in Table 4 that the ZI for pure Cur and Lim (aqueous media) were comparatively less in the free state, showing that by themselves, they have less activity against the bacteria. The values of ZI for coated Fe_3O_4 are represented in Table 4(b). It was observed that there is a synergistic increase in the antibacterial activity of the drugs Cur and Lim when loaded on Fe_3O_4-Dex. The zones of inhibition confirm the bactericidal activity of the drug-coated Fe_3O_4. It is assumed that the coated Fe_3O_4 are stable in the bio medium, which further stabilizes the drug-loaded onto them. Therefore, the retention time between the stable coated Fe_3O_4 and the bacterium increases, modulating the bacterial proteins and thus arresting bacterial growth in agreement with the literature [1]. Thus, it was concluded that by using the combination of biocompatible coated Fe_3O_4 along with the plant-derived drugs, there was enhanced antimicrobial activity. The study says that the drug dosage required for any illness can be decreased by this method as the drug is entirely released at the site of infection by using an external magnetic field [8]. This proves that drug-loaded- Fe_3O_4 dramatically enhances the activity of the drug and can act as a good drug carrier.

3.6. *Drug entrapment efficiency (% EE)*

The amount of drug Cur and Lim loaded on Fe_3O_4 was measured as Drug Entrapment Efficiency (% EE) [10] using a UV-Vis spectrophotometer (Thermo Scientific Evolution 201) in the range of 200 to 800 nm. A solution of a known quantity of Cur and Lim was prepared in ethanol, as mentioned in the experimental section. To this, a known amount of Fe_3O_4-Dex was added. The dispersion was stirred for 45 min, allowed to stand for 10 min, and then coated compounds were separated. Spectra of the solution which contained the unadsorbed Cur and Lim was recorded before and after the adsorption process. The % EE values calculated, the values are given in Table 5, and the UV-Vis spectra are shown in Fig. 6.

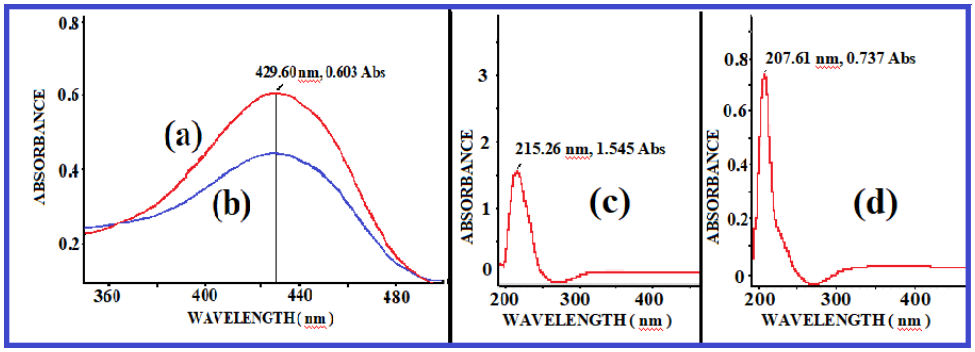

Fig. 6. UV-Vis Spectra of nanoconjugates 1 [Cur a) before adsorption, b) after adsorption on Fe-Dex-Cur 2] Lim, c) before adsorption, and d) after adsorption for Fe-Dex-Lim.

Table 5. EE (%) value for a) Curcumin and c,d) D-limonene on Fe_3O_4-Dextrin conjugates.

Sample	λ_{max} after adsorption (nm)	Intensity before the drug absorption	Intensity after the drug absorption	Entrapment efficiency (%)	Recovered drug (%)
Fe_3O_4- Dex-Cur	428.65	0.603	0.440	27.18	72.96
Fe_3O_4-Dex-Lim	207.61	1.063	0.737	31.25	69.33

In Fig. 6, for Fe-Dex-Cur, the λ_{max} absorbance band at 429 nm is assigned to the n-π^* transition of the chromophore group of curs and is responsible for its yellow color. In Fe-Dex-Lim, λ_{max} absorbance band at 215 nm is due to π-π^* transition. This indicates that the chromophore group does not play a role, and the free -OH group of Cur and Lim was responsible for conjugation. Both peaks matched with literature data [24]. After the adsorption process, the absorption peak intensity decreases, indicating that some amount of the drug is adsorbed on the Fe_3O_4-Dex conjugates. As seen from the spectra, there was good adsorption of all the drugs on Fe_3O_4-Dex. This indicates that the drugs were encapsulated onto Fe-Dex conjugates, with relatively high % EE values, which is due to strong hydrophobic interaction between the plant drugs and the Fe-Dex conjugates. Therefore, these Fe_3O_4 could act as Drug Carriers.

5. Conclusion

In this investigation, we have explored plant-derived drug-loaded functional Fe_3O_4 nanoparticles as a base for enhanced antibacterial therapy, with potential advantages in the field of nano-biomedicine. All the Fe_3O_4 nanocomposite materials viz. Fe_3O_4, Fe_3O_4-Dex, Fe_3O_4-Dex-Cur and Fe_3O_4-Dex-Lim were successfully synthesized by modified co-precipitation method and characterized by modern techniques. XRD study has revealed the particle size to be in nanoparticle range and their high purity. FTIR techniques proved the presence of coatings and secondary shell drug coatings on the Fe_3O_4 magnetic nanoparticles. Magnetic susceptibility (Ms) values were calculated based on VSM studies

indicating the material's superparamagnetic nature. TEM images ensured that the particles were spherical, monodispersed, and in the range of 4.5 to 13 nm. The antimicrobial activity was studied using plant drugs Cur and Lim which were loaded on the synthesized Fe_3O_4-Dex compounds. The drugs showed inhibition zones on the microorganisms with enhanced activity. Fe_3O_4-Dex-Cur and Fe_3O_4-Dex-Lim proved to be efficient for stabilizing and controlling the release of these drugs; thus, maximizing their biological activity and loading the concentration of the drugs can also be controlled. Thus, this study suggests a suitable approach for developing new alternative strategies for enhancing the activity of therapeutic agents for Drug Delivery.

Acknowledgment

Acknowledge S. Mandrekar and M. D'Souza for assisting in experimental work. Department of Microbiology, St. Xavier's College, Goa; SAIF- IIT, Madras; SAIF-IIT, Mumbai; USIC–Goa University; National Institute of Oceanography (XRD Section), Dona Paula, Goa.

References

1. D. Dorniani, A. U. Kura, S. H. Hussein-Al-Ali, M. Z. B. Hussein, S. Fakurazi, A. H. Shaari, and Z. Ahmad, Sci. World J. **2014**, ID 416354 (2014). https://doi.org/10.1155/2014/416354
2. J. Xie, S. Lee, and X. Chen, Adv. Drug Deliv. Rev. **62**, 1064 (2010). http://doi.org/10.10.16/j.addr.2010.07.009
3. T. K. Mandal, and V. Patait, J. Sci. Res. **13**, 299 (2021). https://doi.org/10.3329/jsr.v13i1.47690
4. A. V. V. Nikezić, A. M. Bondžić, and V. M. Vasić, Eur. J. Pharm. Sci. **151**, ID 105412 (2020). http://doi.org/10.1016/j.ejps.2020.105412
5. H. A. Adeola, S. Sabiu, T. A. Adekiya, and R. T. Aruleba, Heliyon, **6**, ID e04890 (2020). https://doi.org/10.1016/j.heliyon.2020.e04890
6. A. Akbarzadeh, M. Samiel, and S. Davaran, Nanoscale Res. Lett. **7**, 144 (2012). https://doi.org/10.1186/1556276X-7-144
7. L. Shen, B. Li, and Y. Qiao, Materials, **11**, 324 (2018). https://doi.org/10.3390/ma11020324
8. I. Liakos, A. Mihai, and A. M. Holban, Molecules, **19**, 12710 (2014). http://doi.org/10.3390/molecules190812710
9. A. M. Grumezescu, M. C. Gestal, A. M. Holban, and L. Grumezescu, Molecules, **19**, 5013 (2014). https://doi.org/10.3390/molecules19045013
10. H. Yin, H. Zhang, and B. Liu, Acta Biochim. Biophys. Sin. **45**, 634 (2013). http://doi.org/10.1093/abbs/gmt063
11. J. A. Lopez, F. Gonzalez, G. Zambrano, and F. Bonilla, Revista Latinoamericana de Metalurgiay Mater. **30**, 60 (2010).
12. K. M. Gregorio-Jauregui, M. G. Pineda, J. E. Rivera-Salinas, and G. Hurtado, J. Nanomat. **8**, 813958 (2012). https://doi.org/10.1155/2012/813958
13. L. D. Tran, N. M. T. Hoang, and T. T. Mai, Colloid. Surf. A: Physicochem. Eng. Asp. **371**, 104 (2010). https://doi.org/10.1016/j.colsurfa.2010.09.011
14. Y Cao, M. Gao, C. Chen, and A. Fan, Nanotechnology, **26**, ID 115101 (2015). https://doi.org/10.1088/0957-4484/26/11/115101
15. M. Khalkhali, K. Rostamizadeh, S. Sadighian, and F. Khoeini, DARU J. Pharm. Sci. **23**, 45 (2015). http://doi.org/10.1186/s40199-015-0124-7

16. E. Rasouli, W. J. Basirun, M. Rezayi, and K. Shameli, Int. J. Nanomed. **13**, 6903 (2018). https://doi.org/10.2147/IJN.S158083
17. N. Liao, M. Wu, F. Pan, and J. Lin, Sci. Rep. **6**, ID 18746 (2016). https://doi.org/10.1038/srep18746
18. C. S. Ciobanu, E. Andronescu, and L. Pall, Rev. Chim. Bucharest, **61**, 231589982 (2010).
19. S. H. Hussein-Al-Ali, M. E. Zowalaty, and A. U. Kura, Biomed. Res. Int. **2014**, ID 651831 (2014). http://dx.doi.org/10.1155/2014/651831
20. D. Predoi, Dig. J. Nanomater. Bios. **2**, 169 (2007).
21. J. F. de Carvalho, I. M. de Azevedo, K. B. Ferreira Rocha, A. C. Medeiros, and A. D. S. Carriço, Acta Cir. Bras. **32**, 46 (2017). http://dx.doi.org/10.1590/s0102-865020170106
22. F. Lin, W. Chen, Y. Liao, R. Doong, and Y. Li, Nano Res. **4**, 1223 (2011). https://doi.org/10.1007/s12274-011-0173-2
23. J. Chetia1, L. R. Saikia, S. Upadhyaya, E. Khatiwora, and A. Bawri, J. Sci. Res. **13**, 195 (2021). https://doi.org/10.3329/jsr.v13i1.47322
24. R. Kitture, S. Ghosh, P. Kulkarni, and X L Liu, J. Appl. Phys. **111**, ID 064702 (2012). http://doi.org/10.1063/1.3696001